Homogeneous Nucleation in Water in Microfluidic Channels

Keita Ando* and Ai-Qun Liu†
School of Electrical and Electronic Engineering, Nanyang Technological University, Singapore 639798, Singapore
Claus-Dieter Ohl
School of Physical and Mathematical Sciences, Nanyang Technological University, Singapore 637371, Singapore
(Received 13 March 2012; published 24 July 2012)

It has been an experimental challenge to test the rupture of liquids with homogeneous nucleation of vapor bubbles. Many prior studies suffered from the ubiquitous presence of impurities in liquids or at container surfaces that spontaneously nucleate and grow under tension. Here, we propose a microfluidic approach to eliminate such impurities and obtain homogeneous bubble nucleation. We stretch the liquid dynamically via the interaction between a laser-induced shock and an air-liquid interface in a microchannel. Reproducible observations of the nucleation of vapor bubbles are obtained, supporting our claim of homogeneous nucleation. From comparisons of the distribution of vapor cavities with Euler flow simulations, the nucleation threshold for water at room temperature is predicted to be −60 MPa.

DOI: 10.1103/PhysRevLett.109.044501 PACS numbers: 47.40.Nm, 47.55.dd, 47.55.dp

Testing the tensile strength of a pristine liquid (the most negative pressure before it ruptures) requires the realization of homogeneous nucleation [1]. However, in practice, heterogeneous nucleation at impurities or container surfaces most likely dominates a cavitation inception process [2,3] and gives rise to a significant reduction of the tensile strength. The measurement of cavitation inception pressure under static conditions originates in the work of Berthelot in which water filled into a glass tubes was stretched on isochoric cooling. Many researchers followed this quasistatic method to determine the cavitation inception pressure, with measured values much less negative than homogeneous nucleation theories predict [4]. One exception is the mineral inclusion experiment [5] in which a much smaller amount of water was trapped in micron-sized fractures of crystals and then stretched according to the Berthelot procedure. Their measured values were scattered possibly due to heterogeneous nucleation, but one measurement showed −140 MPa at 42 °C, which is close to the homogeneous nucleation limit from the classical theory.

Since quasistatic methods demand long observation periods with a high probability of finding nucleation sites from impurities, one may choose dynamic stretching in order to reduce the likelihood of heterogeneous nucleation. Experiments on ultrasonically induced cavitation with careful preparations of the sample water [6–8] obtained reproducible cavitation inception with a threshold pressure around −30 MPa, which is one of the most negative values among acoustic methods. Another way to dynamically stretch the liquid is through shock reflection from free surfaces [4]. Photographic observations of rupturing water near a free surface [9] are particularly useful, but a large volume of water was used in these experiments so that heterogeneous nucleation is unavoidable.

In this Letter, the process of dynamically rupturing water via the interaction between a laser-induced shock and a free surface is explored in a microfluidic channel. As we will present, the use of only very small volumes of water in a microchannel, while studying the process in the nanosecond range, can lead to a significant reduction in heterogeneous nucleation sites. The cavitation inception pressure is determined from comparisons with Euler flow simulations.

The experimental setup consists of a microfluidic channel and an optical system for visualizing the rupture of water as depicted in Fig. 1. Air-saturated, deionized water at room temperature (20 °C) is partially filled in a polydimethylsiloxane (Sylgard 184, Dow Corning) channel of

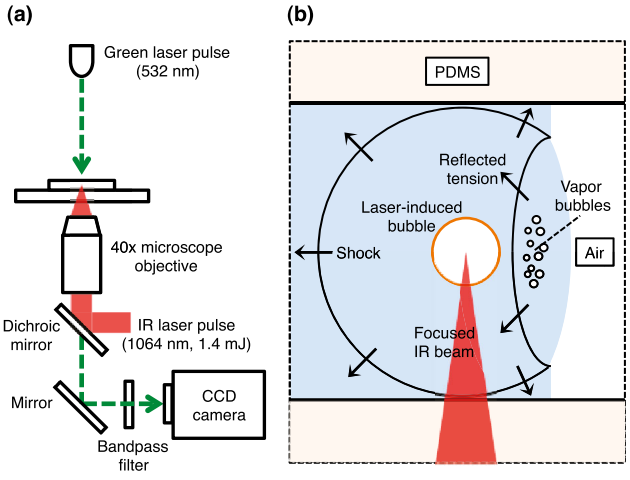

FIG. 1 (color online). Schematic of the experimental setup. (a) The optical system for observing laser-induced phenomena in a liquid-filled microchannel. Images from the top view are captured using a CCD camera. (b) Side view of the interaction of the laser-induced shock with a free surface.

170 μm height and 400 μm width; the chip is mounted on an inverted microscope (IX71, Olympus). The contact angle of the polydimethylsiloxane is approximately 90° so that the resulting air-water free surface is fairly flat. An Nd:YAG laser (Orion, New Wave Research) is used to create single laser pulses at wavelengths of 532 nm (green) and 1064 nm (infrared or IR) with 7.5 ns duration. As the IR laser pulse of 1.40 ± 0.05 mJ energy (the $\pm$ sign denotes a standard deviation from 10 measurements) is focused into the middle of the water-filled channel through a microscope objective ($40\times$, NA $= 0.8$), a spherical shock wave is created due to the rapid expansion of plasma formed within the focal volume after the optical breakdown [10]. After the plasma recombines, a spherical cavitation bubble arises from the localized heat deposition. The spherical shock will eventually reach the free surface and the reflected tension wave can induce the rupture of the water, which is detected from the nucleation of vapor bubbles. Images from the top view of the channel are captured using a CCD camera (pixelfly qe, pco.) with a single exposure of the green laser pulse. A bandpass filter at a wavelength of 532 nm (FL532-3, Thorlabs) is used to protect the camera from the intense laser light. A delay in the illumination is controlled by varying the optical path length of the green laser beam using optical fibers, with respect to the optical breakdown.

The evolution of the laser-induced shock and bubble is first examined without interactions of the shock with channel walls and free surfaces. Here, a water droplet on a microscope slide (instead of water-filled channels) is used as the sample liquid. To ensure the spherical symmetry of the laser-induced phenomena, the IR laser pulse is focused sufficiently away from any boundaries. Figure 2(a) shows the images of the laser-induced shock and cavitation bubble at different times after the optical breakdown. The bright spot in the center of the bubble is due to emission from the plasma. The rapidly expanding plasma accelerates the liquid outward, leading to the formation of a spherical shock whose wave front is identified as a dark fringe in these images. The shock front and the bubble wall are fitted to circles, and their evolution (with the standard deviation of 6 distinct measurements) is plotted in Fig. 2(b). Since the shock and the bubble are fairly spherical, the fitting error is small compared to the one associated with the laser energy fluctuations. It is confirmed that the shock-induced phenomena are reproducible between different experimental runs.

To infer the pressure distribution from the measured evolution, we compare the experiment with simulations. Therefore, multicomponent Euler equations (two-dimensional with azimuthal symmetry), which govern the shock dynamics in compressible fluids, are numerically solved using a finite volume method. Care is taken for accurate shock and interface capturing [11]. In the simulation, interfaces represented by the discontinuity in

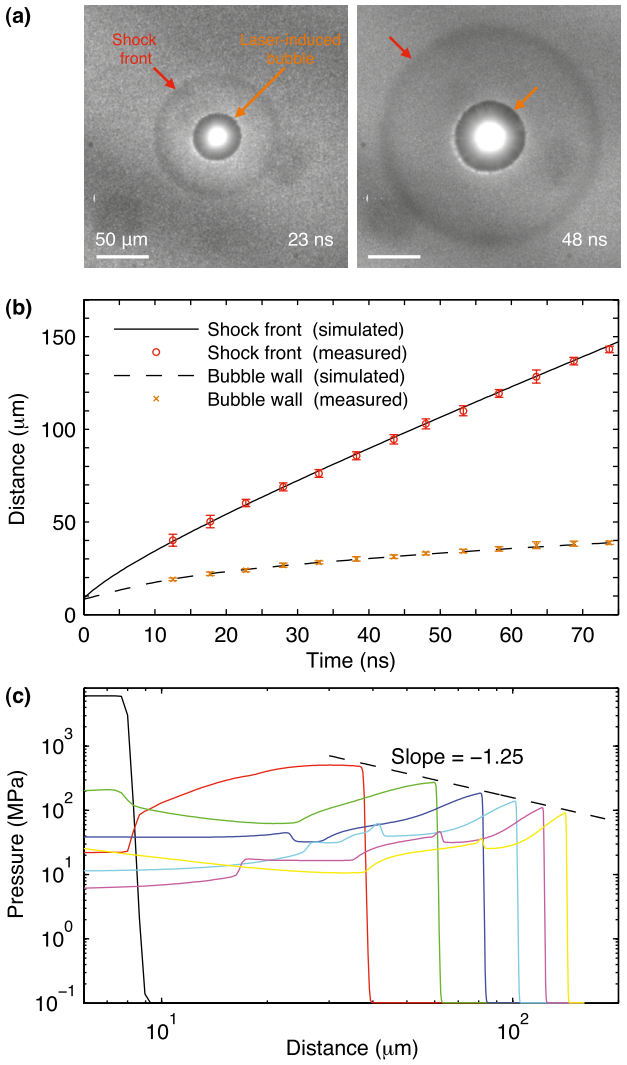

FIG. 2 (color online). Evolution of the laser-induced phenomena. (a) Images of the laser-induced shock and cavitation bubble at different times after the optical breakdown. (b) Temporal evolution of the shock front and the bubble wall. The error bar denotes the standard deviation of 6 distinct measurements. (c) Spatial evolution of the simulated shock pressure 0, 12, 24, 36, 48, 60, and 72 ns after the breakdown.

properties across different fluid components are advected to determine the positions of the air-water interface and the laser-induced bubble wall. For simplicity, the effects of surface tension and phase changes at the bubble wall are assumed to be negligible, and the plasma and vapor phases are treated as perfect gases. The thermodynamic state of water is described by the stiffened equation of state [12], which reduces to the Tait equation of state [13] along an isentrope. Note that calculations of the state of a metastable liquid (whose pressure is below vapor pressure) can vary between different equations of state but these variations within the metastability of concern (away from the spinodal) are minor compared to the experimental uncertainties [8]. The initial state of the laser-induced bubble is given by

adiabatic compression from the undisturbed state of (non-condensible) vapor at 20 °C, for the plasma expands adiabatically [14]. See [15] for details of the numerical setup.

Figure 2(b) compares the measured evolution to the simulation result with an initial bubble radius of 8 μm and a bubble pressure of 6 GPa. The result confirms that the simulation with an appropriate choice of the initial conditions can nicely reproduce the experiment. In Fig. 2(c), the corresponding pressure field at different times after the breakdown is plotted as a function of the distance x from the center of the laser-induced bubble. The peak pressure in this range is found to show a faster decay rate ($x^{-1.25}$), compared to the linear case with a decay rate (x^{-1}). It is emphasized that the axisymmetric flow assumptions within the microfluidic channel are no longer valid once the shock wave reaches the channel walls, i.e., 40 ns after the optical breakdown. Nonetheless, the flow near the laser-induced bubble can still be predicted for a longer time, i.e., till the reflected waves contaminate the flow of interest.

Now, the shock interaction with a free surface and the subsequent bubble nucleation are studied. The distance from the center of the laser-induced bubble to the free surface is 75 μm. Following the simulation in Fig. 2(c), the shock pressure just before reflection is approximately 200 MPa. Figure 3(a) presents the flow configuration from the axisymmetric Euler flow simulation 58 ns after the optical breakdown. The same initial condition for the laser-induced bubble as in Fig. 2 is employed in the simulation, but now with a free surface. The upper and lower half planes show the distributions of the instantaneous pressure and the minimum pressure encountered during the computation, respectively. The positions of the bubble wall and the free surface are also superimposed onto this plot. It is observed that the shock reflects at the free surface as a tension wave due to acoustic impedance mismatch [3,13] while the free surface is deformed by the shock loading. Unless the water ruptures, negative pressures down to −100 MPa will be attained from the passage of the tension wave. It is also interesting to point out that the superposition of the incoming shock and the reflected tension leads to less negative pressure in the liquid close to the free surface.

This simulation is compared with the experimental picture as shown in Fig. 3(b). The water ruptures with the nucleation of small vapor bubbles in a small region next to the gas-liquid interface only. The nucleated bubbles are up to 1 μm approximately (see [15]). Growth to visible sizes is expected to occur nearly instantaneously as the characteristic time for nucleation of these bubbles under a stepwise pressure change (e.g., from 0.1 to −100 MPa) is only a few nanoseconds [2]. In Fig. 3(c), the contour lines for the minimum pressure as well as the simulated interface positions are superimposed onto the image. Even though the displacement effect due to the vapor bubbles is not accounted for in the modeling, the interface positions are accurately simulated. This indicates that the resulting volume fraction of the bubbles is not high enough to disturb the simulation result of the interface positions. These nucleated bubbles can be found within the contour line for the minimum pressure of −60 MPa. Thus, the cavitation inception pressure is approximately −60 MPa. Note that the pressure field within a cloud of nucleated bubbles will deviate significantly from the noncavitating solution because of the dynamics of the bubble cloud [16].

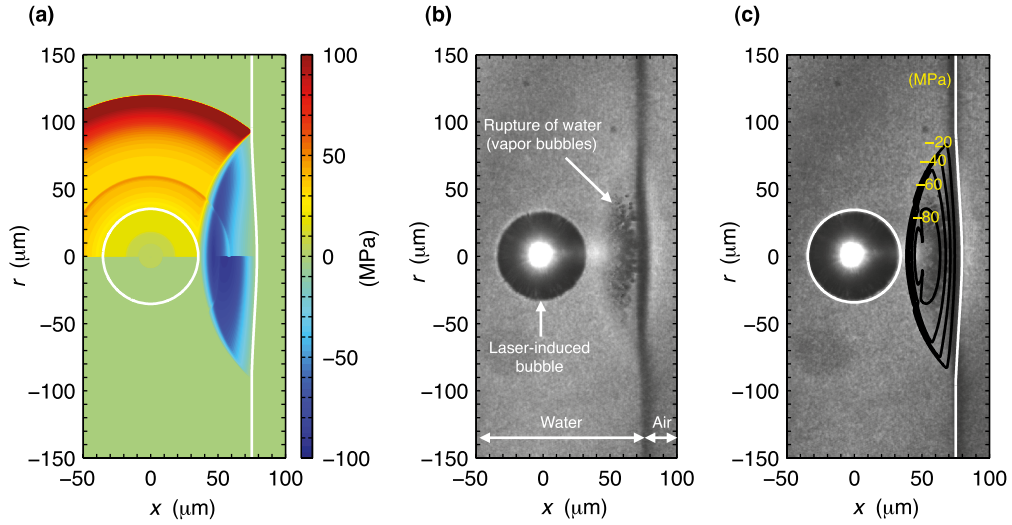

FIG. 3 (color online). Rupture of air-saturated water in the microchannel. (a) Simulated pressure distributions 58 ns after the optical breakdown 75 μm away from the free surface. The upper and lower half planes show the distributions of the instantaneous pressure and the minimum pressure encountered during the computation, respectively. (b) An example of the image of the nucleation of submicron vapor bubbles in the water. (c) Contour lines of the minimum pressure (as well as the simulated interface positions) superimposed onto the image.

The rupture of water 74 ns after the optical breakdown is shown in Fig. 4 while the distance of the laser focus from the free surface is maintained at 75 μm. The axisymmetric flow simulation [Fig. 4(a)] shows that the tension wave, reflected from the free surface, reaches the expanding laser-induced bubble and has now reflected as a compression wave. Due to the wave interaction with the laser-induced bubble, the bubble tends to elongate toward the free surface in the simulation. Now that the liquid is subjected to the tension wave for a longer period, the cavitating region has extended as seen in Fig. 4(b) [in comparison to Fig. 3(b)] and some of the nucleated bubbles have grown into bubbles of a few microns (see [15]). A comparison between the simulation and the experiment [Fig. 4(c)] indicates that the interfaces are accurately simulated and the nucleated bubbles are again found within the contour line for the minimum pressure of -60 MPa. Supplemental Material [15] supports that the nucleation phenomenon is highly repeatable; the nucleated bubbles are always found inside the contour line for the numerically predicted minimum pressure of -60 MPa. The error in fixing the threshold pressure to encompass all bubbles to be inside the respective contour region is estimated to be approximately 5 μm, which relates to an uncertainty in the nucleation threshold of 5 MPa. It follows that impurities or weaknesses of the liquid such as particulate contamination or stabilized gas bubbles are not contributing to such reproducible nucleation. These repeatable observations suggest homogeneous nucleation in the water with a threshold pressure of -60 ± 5 MPa. To date, this is the most negative value reported for dynamic measurements in water.

The current measurement is compared with other acoustic measurements and the classical theory. The extent of the water under tension is now estimated as $(V\tau)^{-1} \approx 10^{11}$ mm^{-3} s^{-1} (where V is defined as the volume of the cavitating region and τ is the characteristic time inferred from the shock width), while the experiments from [6–8] have similar values of $(V\tau)^{-1}$ but show the lower threshold pressure of approximately -30 MPa. The corresponding homogeneous nucleation threshold for water is predicted at -190 MPa from the classical continuum theory [6] with surface tension 72 mN/m. At this threshold, the radius of the nucleated bubbles is approximately 0.8 nm so that the nucleation process in water may not be properly treated with the continuum assumption. This may account for the discrepancy between the theory and these measurements [17].

To demonstrate the applicability of this method for other liquids, the rupture of ethanol is studied [15]. As in the water cases, ethanol at room temperature is partially filled in the microchannel and its dynamic rupture is observed. Now that the contact angle is close to 0°, the resulting air-ethanol free surface has a spherical shape. This case may still be simulated with the axisymmetric flow assumption. Here, we observe cavitation inception at approximately -30 MPa, while the classical theory (with surface tension 22 mN/m [18]) predicts the threshold pressure of -33 MPa and the nucleated bubble radius of 1.4 nm. This agreement suggests that the continuum assumption can be applied to homogeneous nucleation in such a low-surface-tension liquid, as demonstrated in [17].

In this Letter, the dynamic rupture of water has been investigated using a microfluidic approach. Such a small-scale method is shown to be useful for reducing the probability of having heterogeneous nucleation sites and therefore yields the reproducible observation of homogeneously nucleated vapor bubbles in the liquid. Comparisons of the distribution of the nucleated bubbles with the Euler flow simulations lead to an estimate of the cavitation inception pressure of -60 ± 5 MPa for water at room temperature.

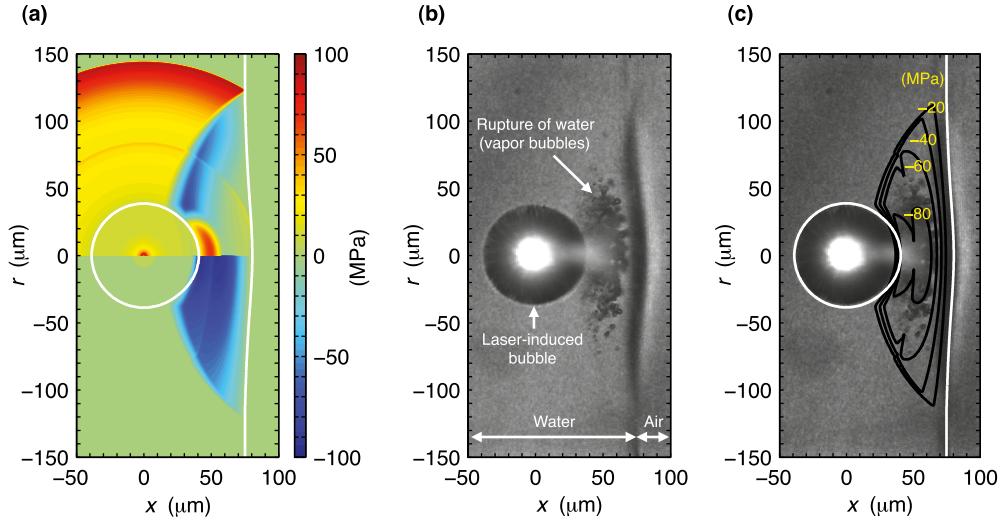

FIG. 4 (color online). Rupture of the water at a later time. (a)–(c) The same experimental and numerical configurations as in Fig. 3, but 74 ns after the optical breakdown.

The authors thank E. Johnsen and H. Gao for helpful discussions. This project was supported by Singapore funding agencies A*STAR (Grant No. 102-171-0159) and EWI (Grant No. MEWR C651/06/171).

*Present address: Department of Mechanical Engineering, Keio University, Yokohama 223-8522, Japan.
†eaqliu@ntu.edu.sg

[1] V. P. Skripov, *Metastable Liquids* (Wiley, New York, 1974); P. G. Debenedetti, *Metastable Liquids* (Princeton University, Princeton, NJ, 1996).
[2] C. E. Brennen, *Cavitation and Bubble Dynamics* (Oxford University, New York, 1995).
[3] T. G. Leighton, *The Acoustic Bubble* (Academic, New York, 1994).
[4] D. H. Trevena, J. Phys. D **17**, 2139 (1984).
[5] Q. Zheng, D. J. Durben, G. H. Wolf, and C. A. Angell, Science **254**, 829 (1991).
[6] E. Herbert, S. Balibar, and F. Caupin, Phys. Rev. E **74**, 041603 (2006).
[7] K. Davitt, A. Arvengas, and F. Caupin, Europhys. Lett. **90**, 16 002 (2010); K. Davitt, E. Rolley, F. Caupin, A. Arvengas, and S. Balibar, J. Chem. Phys. **133**, 174507 (2010).
[8] A. Arvengas, K. Davitt, and F. Caupin, Rev. Sci. Instrum. **82**, 034904 (2011).
[9] V. K. Kedrinskii, Acta Astronaut. **3**, 623 (1976); P. R. Williams, P. M. Williams, and S. W. Brown, J. Phys. D **30**, 1197 (1997).
[10] A. Vogel, S. Busch, and U. Parlitz, J. Acoust. Soc. Am. **100**, 148 (1996).
[11] E. Johnsen and T. Colonius, J. Comput. Phys. **219**, 715 (2006); J. Acoust. Soc. Am. **124**, 2011 (2008).
[12] F. Harlow and A. Amsden, Los Alamos National Laboratory Monograph LA-4700, 1971.
[13] P. A. Thompson, *Compressible-Fluid Dynamics* (McGraw-Hill, New York, 1972).
[14] F. Aitken, F. M. J. McCluskey, and A. Denat, J. Fluid Mech. **327**, 373 (1996); P. K. Kennedy, D. X. Hammer, and B. A. Rockwell, Prog. Quantum Electron. **21**, 155 (1997).
[15] See Supplemental Material at http://link.aps.org/supplemental/10.1103/PhysRevLett.109.044501 for detailed information on numerical methods and supporting experiments.
[16] L. d'Agostino and C. E. Brennen, J. Fluid Mech. **199**, 155 (1989); D. Fuster and T. Colonius, J. Fluid Mech. **688**, 352 (2011).
[17] A. Arvengas, E. Herbert, S. Cersoy, K. Davitt, and F. Caupin, J. Phys. Chem. B **115**, 14 240 (2011).
[18] F. A. M. M. Gonçalves, A. R. Trindade, C. S. M. F. Costa, J. C. S. Bernardo, I. Johnson, I. M. A. Fonseca, and A. G. M. Ferreira, J. Chem. Thermodyn. **42**, 1039 (2010).